M. Sanalatii, P. Herzog, R. Guillermin, M. Melon, N. Poulain and J.-C. Le Roux, "Estimation of Loudspeaker Frequency Response and Directivity Using the Radiation-Mode Method," *J. Audio Eng. Soc.*, vol. 67, no. 3, pp. 101–115, (2019 March.).
DOI: https://doi.org/10.17743/jaes.2019.0001

Estimation of Loudspeaker Frequency Response and Directivity Using the Radiation-Mode Method

MARYNA SANALATII[1, 2, 3], PHILIPPE HERZOG,[1] *AES Member*, RÉGINE GUILLERMIN[1],

MANUEL MELON,[2]* *AES Member*, NICOLAS POULAIN[3], AND JEAN-CHRISTOPHE LE ROUX[3]
(manuel.melon@univ-lemans.fr)

[1]*Laboratoire de Mécanique et d'Acoustique (LMA), UMR CNRS 7031, 4 impasse Nikola Tesla, CS 40006, 13000 Marseille, France*
[2]*Laboratoire d'Acoustique de l'Université du Mans (LAUM), UMR CNRS 6613, Av. Olivier Messiaen, 72085 Le Mans Cedex 9, France*
[3]*Centre de Transfert de Technologie du Mans (CTTM), 20 rue Thalès de Milet, 72000 Le Mans, France*

This paper proposes the radiation mode method to estimate the frequency response and directivity pattern of loudspeaker systems. The underlying theory and method principle are described first. The method is then assessed in both an anechoic room and large non-anechoic hall by measuring four loudspeaker systems featuring different radiation patterns. Results show a satisfactory level of accuracy for the proposed method across all sources tested and both measurement rooms, especially when considering the reduced number of measurement points needed. These examples are then complemented by a preliminary parametric study based on the simulation of a tall system, namely a line array for which standard measurement techniques are not applicable. More specifically, the influences of identification point locations, noise, and RM series truncation are all investigated. The output of these simulations illustrates the potential of this method to characterize sound sources that cannot be measured using classical means.

0 INTRODUCTION

The acoustic radiation of common loudspeaker systems can be easily measured using modern measurement techniques. The measurement process, however, requires free-field conditions that may be difficult to satisfy by manufacturers: large anechoic rooms are very expensive and outdoor measurements are subject to uncontrollable weather conditions [1–3].

Moreover, some cases actually prevent the standard methods [4] from yielding reliable results. For instance, directivity patterns, which are a far-field quantity, should be measured at a far enough distance from the source, i.e., typically greater than the source dimensions and/or minimum wavelength. This distance therefore exceeds 4 m for some sound reinforcement systems, especially line arrays (very tall devices) or subwoofers (generating very low frequencies). In such cases, most anechoic rooms are practically useless due to their limited working volume, thus leading to unreliable measurements far from the source—even above the cutoff frequency.

For these reasons, many alternative approaches have been developed in order to allow for measurements under non-anechoic conditions. Among these approaches, windowing or gating of the measured response can be used to remove wall reflections [5–9]. This technique may also be coupled with near-field pressure measurements [2] or with a model for improving results at lower frequencies [10–12].

Another alternative approach to conducting pressure measurements consists of measuring the velocity field on the speaker membrane and on the box, then inputting this measurement data into the numerical radiation computations. Such a step yields exhaustive spatial information yet does require an extensive amount of data to generate reliable results at higher frequencies. These results are also dependent on the adequacy of the loudspeaker mesh in simultaneously representing the vibration and the acoustic fields. Moreover, the velocity field must be measured with a contactless method, e.g., by a scanning laser vibrometer, despite its rather high price. Conversely, the radiated pressure may be easily estimated at lower frequencies by computing the loudspeaker diaphragm velocity by means

* Author to whom correspondence should be addressed (e-mail: manuel.melon@univ-lemans.fr)

of the "Thiele/Small" electroacoustic model [13]. This protocol however is limited to the pistonic behavior of the membrane (typically below 1 kHz), in excluding medium and higher frequencies (at which the actual vibration pattern governs the radiated field) and in not providing any reliable information regarding directivity.

Directivity measurements are particularly demanding. For instance, a full sphere recording, with a 5° angle grid, requires 2522 unique points (or 64442 unique points at a 1° resolution). Such high numbers may be reached using robotized equipment, although the figures do reveal the difficulty involved in obtaining a reliable radiation pattern, especially at higher frequencies where even the 5° resolution may be insufficient.

Fortunately, since the work completed by Weinreich and Arnold [14], several methods based on near-field measurements coupled with far-field extrapolation using a set of mathematical functions have been developed. These approaches generally involve spherical [15–17] or cylindrical [18] harmonic expansions, yielding estimations while significantly reducing the number of measurements, i.e., down to a value correlated with the number of terms in the particular series. However, a dense measurement grid is still needed whenever the situation imposes a high-accuracy directivity pattern. To overcome this drawback, several solutions have been proposed to extrapolate the missing data [19]. The Helmholtz Equation Least Squares (HELS) Method [20] allows relaxing the measurement grid density or symmetries may be introduced in the tested source radiation pattern [18]. In non anechoic rooms, holography based methods have also been proposed to separate the field radiated by the tested source from the field reflected off of the room boundaries by reliance on double layer pressure measurements [3, 21, 18].

This paper proposes using an expansion over the radiation modes (RMs) of the body [22], leading to a method that combines a limited number of pressure measurements with a numerical tool. The outcome then allows estimating both the frequency and angular responses over a wide frequency range. This RM technique also serves as an estimation method based on a 3D expansion of the acoustic field. Compared to the aforementioned free-field expansions, its specificity lies in accounting for diffraction over the source body in the expansion series. The resulting faster convergence of the RM series makes it possible to reduce the number of measurements, in exchange for a preliminary computation of the RMs.

The RM method is applied herein as a means to extrapolate far-field data (which may be difficult to measure) from measurements performed close to the object (see Fig. 1), thus requiring less effort and avoiding the use of an anechoic room. This goal is similar to that pursued in previous work based on equivalent sources [23] yet adds some generality since the explicit use here of the RM series ensures that the method does not depend directly on the tool implemented to determine the RM. This method is first described in Sec. 1. Measurements are then presented for assessing the on-axis responses and directivity patterns of sample loudspeakers in Sec. 2 (some of these measurements have already been presented in previous conference papers [24, 25] but will be discussed here in greater detail). Next, Sec. 3 analyzes a number of RM method properties based on numerical simulations of a line array. Last, Sec. 4 summarizes the specificities of the current method and its limitations.

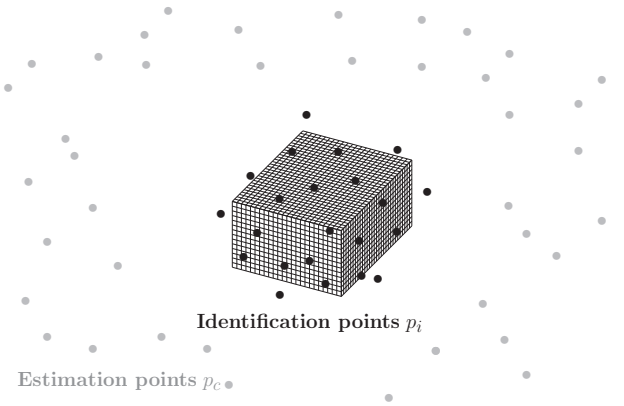

Fig. 1. Sketch showing the potential locations of the identification points (black) and of the estimation points (gray) around a discretized source.

1 THEORY

The RM method has basically been inspired by an inverse acoustic imaging technique first proposed by Veronesi et al., who employed the singular-value decomposition (SVD) to regularize the required inversion process [26]. A similar approach was proposed by Borgiotti et al. [27], who used the SVD to define an orthogonal decomposition of the field radiated by a vibrating body in 3D space [28]. Instead of expanding the propagation operator in open space, Sarkissian then proposed expanding the field over the body surface, leading to decomposition of the radiation impedance [22]. This notion was later used by Elliott and Johnson, who showed the interest of this expansion for active noise control in labeling it "radiation modes" [29]. Compared to the holographic techniques that use an expansion valid for any propagating acoustic field, the RMs are defined for a specific body geometry, which leads to a more efficient expansion, thus requiring fewer terms for a given level of accuracy.

1.1 Radiation Impedance Matrix

Let's consider a body (in this case a loudspeaker box) bounded by its closed surface S and radiating toward the surrounding space Ω. This external radiation problem may be described on S by an acoustic impedance operator $\mathbf{Z_a}$ expressing how the external boundary conditions in Ω react and modify the acoustic pressure on the surface S when vibrating [30]. The operator is defined in continuous space but has no closed-form expression, except in very specific cases. For arbitrary geometries, numerical solutions may be found by discretizing the problem. The surface S is split into a number N_e of sufficiently small elements (i.e., forming

a mesh), and the operator is thereafter approximated by a matrix $\mathbf{Z}$ defined as:

$$\mathbf{p_s} = \mathbf{Z}\ \mathbf{q_s}, \tag{1}$$

where $\mathbf{p_s}$, and $\mathbf{q_s}$ are respectively the vectors of pressures and volume velocities on the various elements of surface S. Note that this relation defines a unique $\mathbf{Z}$ matrix for subspace Ω that remains valid for any vector $\mathbf{q_s}$. Several methods are able to obtain a numerical estimation of the $\mathbf{Z}$ matrix for a given mesh of surface S. The Boundary Element Method (BEM) [31] or Equivalent Source Method (ESM) [32] may both be introduced for this purpose.

The authors have chosen to use a custom research software specifically developed at the LMA Laboratory to compute $\mathbf{Z}$ and suitably expand it for the RM method. A brief description of this software is given in the Appendix for the reader's convenience but not in detail since any alternative method or software could be used to derive the $\mathbf{Z}$ matrix and expand it. The present paper focuses on the RM method itself, regardless of the tool employed to obtain the RMs.

1.2 Radiation-Mode Expansion

Most applications in electroacoustics do not require knowing the acoustic pressure very close to the vibrating surface, i.e., in its near-field. The on-axis pressure or directivity patterns need instead to be estimated in the far-field, as this estimation would significantly reduce the complexity of the radiation problem, since the pressure could be estimated without having to take into account the near-field pressure resulting from evanescent modes [33]. For subsequent calculations, we will therefore only consider the radiation resistance matrix (i.e., the real part of the $\mathbf{Z}$ radiation impedance matrix), as proposed by Sarkissian [22]. This protocol is not highly restrictive: the near-field limit has been estimated to lie fairly close to the vibrating surface even if the far-field situation has not yet been reached [34, 35].

The radiation resistance matrix $\Re(\mathbf{Z})$ can then be expanded using a singular-value decomposition (SVD) [36]:

$$\Re(\mathbf{Z}) = \mathbf{U}\Sigma\mathbf{V}^* \tag{2}$$

where $\mathbf{U}$ and $\mathbf{V}$ are unitary matrices (size $N_e \times N_e$) whose columns are the vectors U_k and V_k corresponding respectively to the pressure and volume velocity for the k-th RM; the * symbol denotes the conjugate transpose, and Σ is a square diagonal matrix (size $N_e \times N_e$) composed of positive real values σ_k proportional to the radiation efficiency of each term. This expression allows expanding any far-field radiation problem over a set of N_e orthogonal solutions on S, hence the name "radiation mode."

The RM series computation is based on a model of diffraction by the source body. The RM series is defined from the radiation matrix and is independent of any (e.g., measured) velocity distribution. The mesh used to compute the RMs does not therefore need to distinguish vibrating parts and rigid parts. Moreover, this mesh is not required to describe small geometric details, a condition leading to a simpler mesh than that required for an accurate radiation computation, which must include the smaller vibrational scales.

Conversely, let's note that $\mathbf{U}$ and $\mathbf{V}$ cannot expand any pressure $\mathbf{p_s}$ and volume velocity $\mathbf{q_s}$ fields on S since they have been defined to expand just the far-field behavior: the proposed expansion is only valid for "large enough" distances (a criterion further analyzed in Sec. 3.3). This approximation allows for a smaller number N of modes, typically less than 100, in order to accurately represent the far-field quantities—especially at lower frequencies (see discussion in Sec. 3.2). This reduction in number of modes significantly reduces the computation time. In sum, the RM method uses an efficient expansion dedicated to the source geometry for estimating its far-field radiation.

1.3 Mode Weighting

The RM series proposed in the previous section is independent of any vibration pattern, loudspeaker layout on the enclosure, etc.; it serves to expand any far-field radiated by the source body, provided each mode k is weighted by a suitable coefficient w_k.

An inversion scheme may therefore be used to identify these weights from pressure measurements performed close to the source, at the so-called "identification" locations P_i (hence the subscript "i"). For this purpose, the transfer function matrix $\mathbf{H_i}$ is computed between the N RMs (considered as vibration patterns) and the N_i pressure field $\mathbf{p_i}$ radiated by this RM at the set of identification points P_i around the tested source. The vector $\mathbf{w}$ of the N weights w_k is then easily obtained by use of a pseudo-inverse of $\mathbf{H_i}$:

$$\mathbf{w} = (\mathbf{H_i}^*\ \mathbf{H_i})^{-1}\ \ \mathbf{H_i}^*\ \ \mathbf{p_i} \tag{3}$$

To build a well-posed inversion problem, the number of identification points should equal or exceed the number N of RMs; hence, selecting this number N is the first step to undertake. A correct N value is also important in ensuring a proper inversion: computing a pseudo-inverse matrix is very fast but may lead to inaccurate results when the condition number of $\mathbf{H_i}$ is high, since this would magnify small measurement errors on p_i. A simple way to cope with this problem consists of truncating the expansion to N RMs, where N is chosen by retaining only the efficient terms. For instance, N may be chosen so that the cumulative sum of the first N values in Σ represents 98% of the sum of all its elements [31] (see Sec. 3.5).

The location of the identification points is also important: they should not be located in the very near-field, where the required number of terms is much greater, nor should they be at a distance too far to maintain a reasonable signal-to-noise ratio. Practically speaking, the required distance is quite small compared to the source dimensions [35], thus enabling pressure measurements at identification points in the vicinity of the enclosure.

1.4 Expansion

When the RM series is known and truncated to N terms, with the corresponding expansion coefficients w_k having been obtained from the identification measurement data,

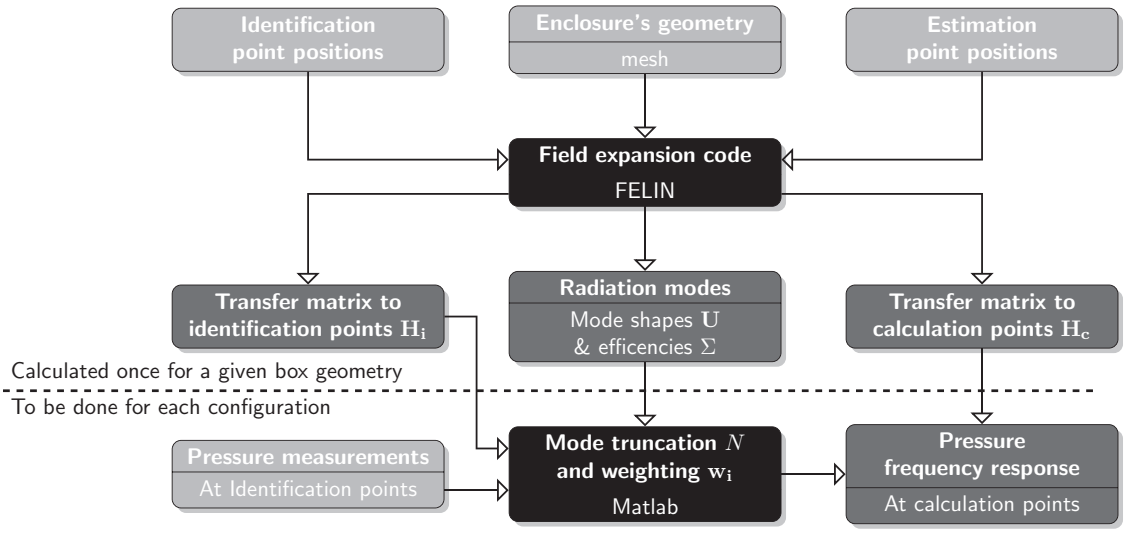

Fig. 2. RM method flowchart—the input data are shown in light gray and output data in dark gray. Numerical calculations are depicted in black

the weighted sum of the RMs acts as a good substitute for the actual vibration pattern—with a far-field radiation close to the actual one.

The last stage of the method consists simply of computing pressures on a set of points P_e chosen in order to obtain the desired responses or directivity patterns, thus leading to an estimation of the actual pressures at these selected locations, hence the subscript "e." Note that the number of such estimation points may be very large, with a marginal CPU cost, and an arbitrary spatial resolution may thus be obtained from the small number of actual measurements. To run this method, the transfer matrix $\mathbf{H_e}$ would need to link the N RM patterns over S to the vector $\mathbf{p_e}$ of the pressures at the target locations P_e:

$$\mathbf{p_e} = \mathbf{H_e}\mathbf{w}, \tag{4}$$

where $\mathbf{w}$ is the weights vector computed using Eq. (3).

A flowchart summarizing the steps required by the RM method is shown in Fig. 2. Note that the computation stage only needs to be performed once for a given box shape, although measurements can be processed for several configurations (different loudspeaker models, locations, filters, etc.).

To further reduce computation time, it may be advantageous to lower the number of frequencies at which the RMs need to be computed. This step becomes especially attractive when the RMs are computed using a BEM method, which must be performed independently at each frequency. Such a drop in CPU time is possible thanks to the fact that the RMs do not change abruptly with frequency, as has been suggested by a number of authors under the name "nesting property" [37]. The basic idea herein is that measurements at all frequencies within a frequency band may be post-processed using the RM series computed at the upper frequency of this band. As an example, when dealing with high-resolution spectra obtained through FFT, using the same RM series for 10 frequencies reduces RM computation time by the same factor of 10, with just a minor loss in accuracy [24].

2 EXPERIMENTAL VALIDATION

The RM method will now be assessed by applying it to actual speaker systems. A subset of these results has been presented in a previous conference paper [25] and will be briefly summarized here.

2.1 Tested Systems

Four distinct systems have been designed for the validation process: two closed-box systems and two subwoofers with different directivities. The closed-box systems have already been described in detail [24, 25]. The subwoofers share a common structure with two identical small bass reflex enclosures tied together. They differ only by their active filter: the first set-up has been designed to obtain a cardioid pattern according to an approach proposed by Boone [38], while the second merely inverts the polarity of one of the two speakers in order to target a figure-of-eight directivity pattern [25]. The four measured systems are briefly listed below:

- SC1 – "Single Closed box 1": bookshelf closed-box system (42 cm× 24 cm× 34 cm) equipped with a Monacor SPH-8M-8 loudspeaker (membrane Ø 22 cm);
- SC2 – "Single Closed box 2": column system (19 cm× 75 cm× 16 cm) equipped with a Fostex FE126En loudspeaker (membrane Ø 9 cm);
- CDR – "Cardioid Dual Reflex": dual reflex subwoofer (79.2 cm× 44.4 cm× 34.4 cm) equipped with two Visaton WS-17E-4 loudspeakers (filter 1);
- BDR – "Bi-directive Dual Reflex": dual reflex subwoofer (79.2 cm× 44.4 cm× 34.4 cm) equipped with two Visaton WS-17E-4 loudspeakers (filter 2).

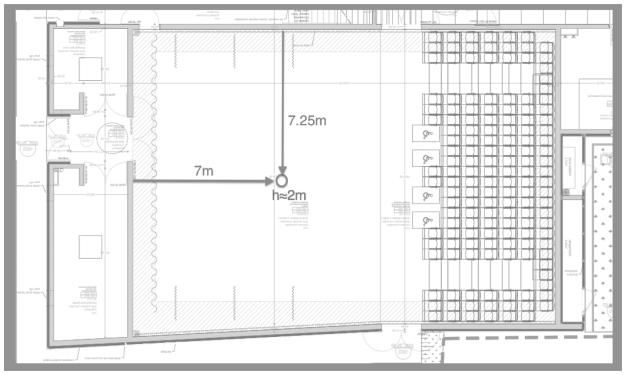

Fig. 3. Large hall layout: the circle shows the position of the tested speaker. Distances to the nearest surfaces are also indicated.

2.2 Measurement Procedure

All systems have been measured in two distinct environments:

- The LAUM anechoic room (working volume 4.9 m $\times$ 3.9 m $\times$ 3.6 m and cut-off frequency of approx. 100 Hz).
- In situ conditions: a large room with characteristics close to those of an industrial hall (gross dimensions $\simeq$ 9 m $\times$ 20.5 m $\times$ 14 m) has been used. The tested source was mounted on a stand 2 m above ground level (see Fig. 3). The room reverberation time gradually decreases from 2.3 s in the 125-Hz octave band to 0.9 s in the 4000-Hz band, yielding critical distances from 1.9 m to 3.3 m, respectively. These values are much higher than the identification point measurement distances (20 or 30 cm).

For all experiments each system was driven by a band-limited white noise signal. Pressure signals were recorded by sequentially placing the same Brüel & Kjær measurement microphone at each measurement location, thus avoiding any calibration issues. Frequency responses (i.e., ratio of the measured pressure to the input voltage) for specific frequencies, with a 16-Hz frequency resolution, were computed using 200 steady-state measurement averages.

2.3 On-Axis Response

The on-axis pressure response at 1 m has been estimated for both the SC1 and SC2 systems. The RM method was applied with 37 (resp. 39) identification points, located 20 cm (resp. 30 cm) from the sources. A conventional measurement of the frequency response was also conducted in the anechoic room and then used as a "reference" measurement. Results are plotted for both rooms in Fig. 4 for SC1 and Fig. 5 for SC2. These figures also include two vertical lines labeled "Box" and "Piston," i.e., corresponding to the frequency limits relative to the mesh sizes of the box and membrane for the two speaker systems.

Figs. 4 and 5 reveal two reference curves with some significant differences. These discrepancies can be explained as follows: measurements in the anechoic room and large room were performed on the same speaker system but at a six-month interval, which accounts for some of the differences. Moreover, measurement uncertainties are not negligible over large distances in an anechoic room. We used a room with non-removable girders, thus creating diffraction effects. Last, the acquisition system and post-processing differed for the two measurement sessions (i.e., a portable system was needed for the large hall) yielding different frequency vectors for the two sessions. Note that each subfigure contains a unique frequency vector, which explains why the reference curve was measured twice, once for each system.

Results obtained by the RM method, computed with the "near-field" measurements under anechoic conditions, are

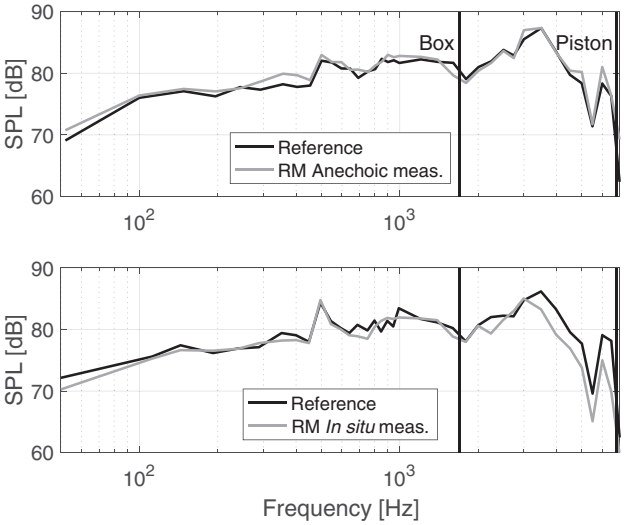

Fig. 4. On-axis sound pressure level for SC1. Upper graph—black: reference, gray: RM method from measurements performed in the anechoic room. Lower graph—black: reference, gray: RM method from measurements performed in the large hall.

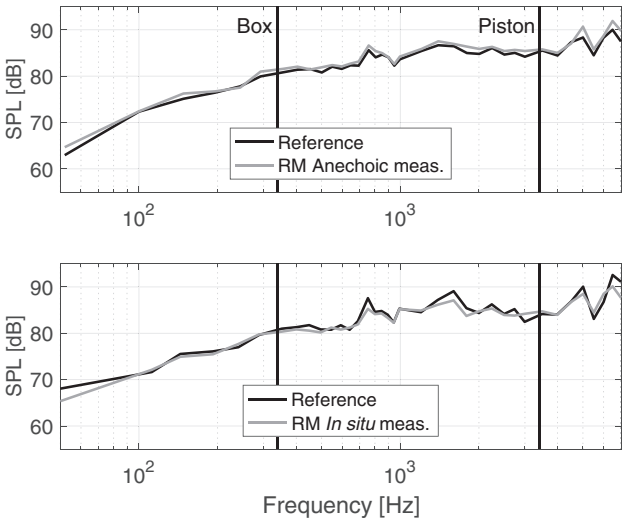

Fig. 5. On-axis sound pressure level for SC2. Upper graph—black: reference, gray: RM method from measurements performed in the anechoic room. Lower graph—black: reference, gray: RM method from measurements performed in the large hall.

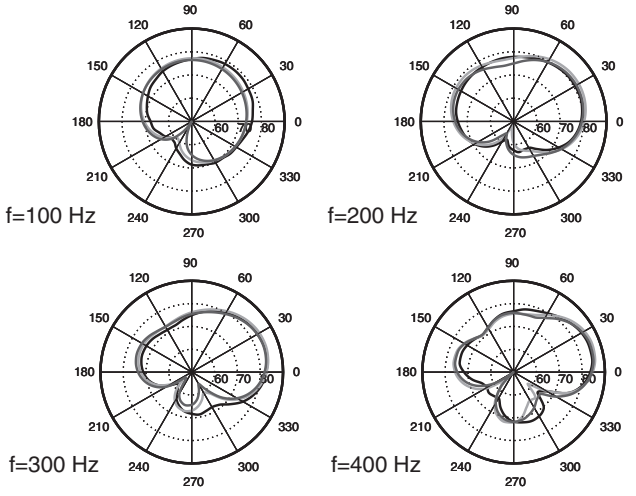

Fig. 6. Comparison of SPL vs. angle at 1 m for the CDR system: reference (black), and computation with the RM method from data measured in the anechoic room (dark gray) or in the large hall (light gray)

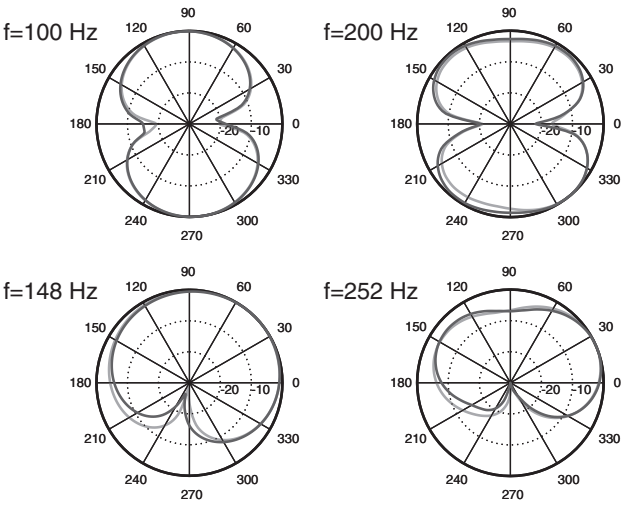

Fig. 7. Upper figures: directivity patterns for BDR at 4 m computed with the RM method from data measured in the anechoic room (dark gray) or the large room (light gray). Lower figures: directivity patterns for CDR at 4 m computed from data measured in the anechoic room (dark gray) or the large room (light gray).

in close agreement with the reference values at most frequencies and for both systems (Figs. 4 and 5, upper graphs). For the RM method computed with the in situ data, results are also reasonably good (Figs. 4 and 5, lower graphs). Note that at some frequencies, discrepancies between reference and RM curves can reach 3 dB, which may be due to anechoic room imperfections, like the aforementioned girders.

A slight underestimation is detected however in the on-axis level for SC1 above 3 kHz as regards the in situ RM estimation. This discrepancy does not seem to be correlated with differences in the model (in fact quite the opposite: the SC2 mesh is much coarser, with 520 elements instead of 5364 for SC1). One possible cause is the larger SC1 speaker membrane, combined with a wider enclosure (compared to the SC2 column), which leads to more directive radiation. For the in situ SC1 measurements, the radiated pressure on the rear face is significantly lower at higher frequencies, thus more easily contaminated by noise and reflections from the walls. For anechoic measurements, the SNR is good even for rear measurements, which in turn yields a good estimation over the full frequency band.

2.4 Directivity Patterns

Directivity patterns have been estimated for both dual reflex sources. The RM method was used with 58 identification points located 30 cm from the sources. Fig. 6 plots the sound pressure levels at 1 m for the CDR source as a function of the angle for three different measurement methods: the reference method and the RM method under both anechoic and in situ conditions.

The three curves are all in reasonably good agreement, although some discrepancies may be observed around angles corresponding to weak radiation. Once again, this observation is the likely result (at least to some extent) of an SNR too low for the measurements close to such locations. Because the RM method is based on an inversion of all measurements as a whole, the local accuracy of the estimation is not directly correlated with the local SNR of the measurement; however, a slight error on the RM weights exerts more influence when all terms must sum to zero than when they combine to build a radiation maximum.

One interesting feature of the RM method is its ability to compute directivity patterns at distances larger than the room size. In our case, the working area of the anechoic chamber is 4.87 m $\times$ 3.87 m, which does not allow for measurements 4 m from the source at the room center. Fig. 7 plots the directivity pattern of BDR and CDR systems at 4 m, as estimated via the RM method. Extrapolations from data measured in the anechoic room or the large hall lie very close to one another for both systems. Although no reference data are available at these distances, the RM-based directivities closely match the anticipated trends, i.e., cardioid for CDR and figure-of-eight for BDR, as long as the wavelength is large enough compared to the source size ($\simeq$ up to 200 Hz).

This last estimation result emphasizes the potential benefit of the RM method, which can accommodate small facilities with effective acoustic treatment, as well as large facilities with substandard acoustic treatment (to a reasonable extent). Another advantage of the RM method is to allow for sparse sampling when measuring a source. The measurements can, for example, be performed using an existing microphone set-up in which the device being tested is inserted for RM identification.

3 SIMULATION OF A LARGE SYSTEM

To further investigate RM method potential, let's now consider a sound reinforcement line array. This source has been chosen by virtue of being very tall, with many radiating surfaces, and producing a highly focused sound field. Moreover, we selected a device with a rather complicated

body shape, i.e., one based on the "Digital and Geometric Radiation Control (DGRC)" principle, which combines digital filters with a "step-array" enclosure shape [39].

In this section no actual measurements will be presented since no suitable facility was available. We therefore used a direct BEM model to compute the identification and reference pressures, considered as "virtual measurements" (VM). These VM were obtained by running the commercial code Sysnoise. An RM estimation could then be derived, as usual, through use of our custom software. This "all-simulation" process yields an accurate computation of the estimation errors and thus indicates the method limitations without the uncertainty of actual measurements.

3.1 Simulated System

The simulated device approximates the Active Audio SA-180 column loudspeaker, featuring 22 individual drivers distributed over 3 tilted faces (see Fig. 8). For these simulations, the steering of the line array is of little importance; we therefore did not use optimized filters but simply imposed a unitary velocity on each of the circular surfaces simulating the loudspeakers. These elements were grouped into three channels, like in the actual passive device, with a delay between channels simply estimated from the geometric shift of the three steps in the front face. Although suboptimal, this set-up leads to a continuous wavefront, in building a sharp directivity, which is the situation we are seeking to analyze. The system has been designed for an installation roughly 2.50 m above ground level, in order to cover an audience placed up to 60 m from the source. No measuring facility would obviously be suitable for such a source, hence the choice to rely on numerical simulations.

We used a direct BEM model containing $N_e = 11268$ triangular elements, with an average size of about 12 mm (thus valid up to around 2 kHz). For direct simulation (VM), the loudspeaker locations are meshed as circular zones on the array face, but the actual loudspeaker diaphragm geometry (cone depth, surround shape, etc.) is not taken into account. This same mesh is then used for the RM identification, although the loudspeaker membranes do not need to be meshed separately for the RM computation.

One specificity of this test case considered here is the presence of the ground, as described by a rigid plane at height $z = 0$, which is included in both the virtual measurements and RM identification. As such, passive scattering objects may also be included in the RM computation (here, by adding an image source) in order to match identification conditions or radiation conditions. Moreover, our far-field target is the pressure over the "ground" (rigid plane), a choice that allows for a more accurate comparison of results (in avoiding comb filtering), despite not being a realistic situation since the line array is designed for a standing audience.

3.2 Field Reconstruction over the Ground

As an initial simulation case, we'll provide here an example of field reconstruction in order to add greater detail regarding the process.

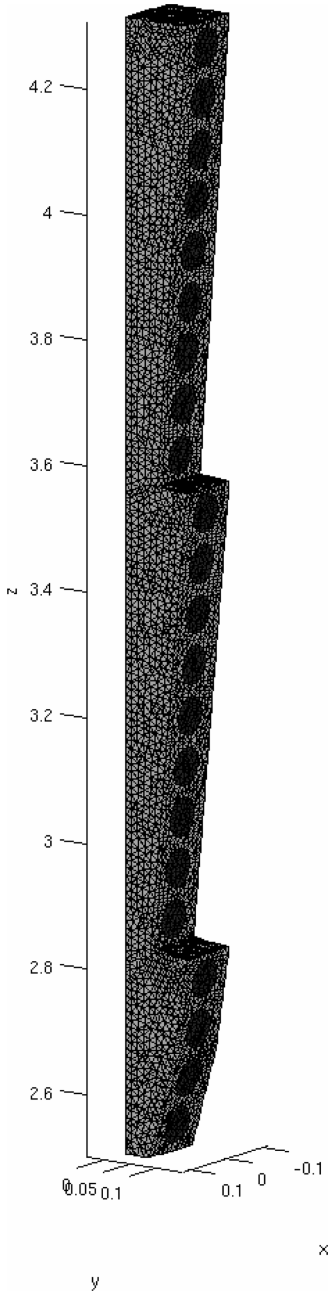

Fig. 8. Step-array mesh—the darker discs correspond to the 22 loudspeakers

Let's begin with a mesh of simplified geometry and suitable element size (for the targeted frequency range); for our purposes here, it is the same mesh used to produce the VM. The next step consists of computing the **Z** matrix and expanding it through an SVD. We used our custom software because such options are not available in commercial codes. Regardless of the tools used to obtain the RMs, they all provide the **U**, **V**, and Σ matrices needed for the method, which starts by selecting the N RMs to be used. This number stems from a tradeoff: like for other expansion methods, the accuracy of results is improved by increasing the number of terms; however, more measurements would then be needed to identify the expansion coefficients. We therefore

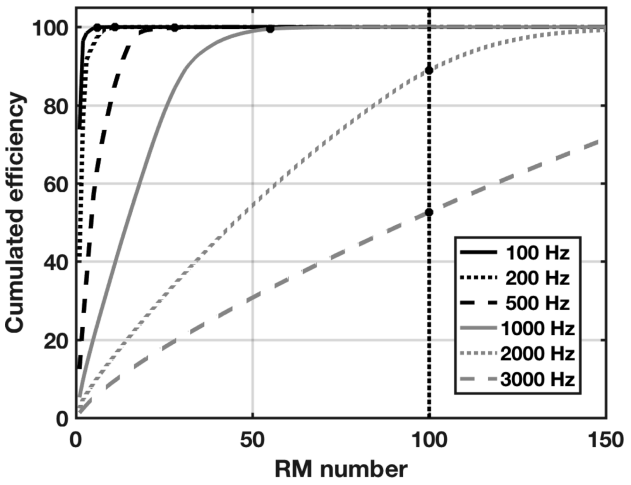

Fig. 9. Cumulative efficiencies as a function of the number of modes for several frequencies

sought to determine a minimum value of N while ensuring "reasonable" accuracy; this choice will be investigated in Sec. 3.5.

The minimum number N_{min} of RMs may be estimated from the Σ matrix, in which each term σ_k is proportional to the radiation efficiency of the RM numbered k, as ranked in decreasing order.

The "cumulative efficiency" CE for order N can then be defined as:

$$CE = \frac{\sum_{k=1}^{N} \sigma_k}{\sum_{k=1}^{N_{max}} \sigma_k} \tag{5}$$

Choosing the most efficient RMs therefore simply consists of selecting N with a high enough CE value. The criterion $CE = 98\%$ has been found to be reasonable for all our examples. Note that in Eq. (5) the denominator value is the sum of all values of Σ, as approximated from the initial N_{max} values. The number N_{max} may be much lower than N_e, since the singular values decrease rapidly with increasing order. For iterative SVD algorithms, CPU time is reduced.

The CE curves are displayed in Fig. 9, which shows a very fast convergence at lower frequencies, where a small number N_{min} of RMs seems sufficient. Conversely, the number of RMs required at 2 kHz would be greater than 150 to reach a cumulative efficiency of 98%. We decided, however, to limit this number to 100 since a large number of RMs entails a significant CPU cost, while 2 kHz is the upper limit anyway for BEM mesh validity. At each computation frequency, the number N_i of identification points was set at twice the number N of RMs selected, hence the transfer matrix can be inverted without regularization. This choice is suboptimal, yet the high fixed N_i/N ratio does avoid tuning a regularization parameter, in simplifying method assessment.

The corresponding identification parameters are summarized in Table 1.

The identification locations must then be determined. Most expansion methods lead to better performance when used with a set of locations adapted to the series terms in order to respect quadrature rules. Such is not an option when using RMs determined numerically for each source geometry. Consequently, the identification locations are selected "evenly" over a surface surrounding the source. This choice is somewhat arbitrary and will be investigated in Sec. 3.3.

For our present example, the identification locations were randomly selected on the surface of a parallelepiped surrounding the source, 10 cm from its surface (surface $C1$, see Table 2). The set of identification locations is therefore sparse and very close to the source surface, thus compatible with an in situ measurement.

Pressure maps are computed on the floor over a 20 m $\times$ 100 m area underneath the array (i.e., 8,241 positions, with an even 50-cm spacing). Figs. 10 and 11 show these maps at four different frequencies in comparing two results: the direct BEM computation, considered here as the

Table 1. Number of RMs used for the SA-180 identification

Freq. (Hz)	100	200	500	1k	2k
N_{min}	6	11	28	55	100
N_i	12	22	56	110	200

Table 2. Geometries (in m) of the three identification surfaces

Set	$C1$	$C2$	$C3$
x_{min}	–0.158	–0.258	–0.358
x_{max}	+0.158	+0.258	+0.358
N_x	5	7	9
y_{min}	–0.100	–0.200	–0.300
y_{max}	+0.216	+0.316	+0.416
N_y	5	7	9
z_{min}	+2.400	+2.300	+2.200
z_{max}	+4.408	+4.508	+4.608
N_z	22	24	26
N_{tot}	370	626	930
D_i	0.1	0.2	0.3

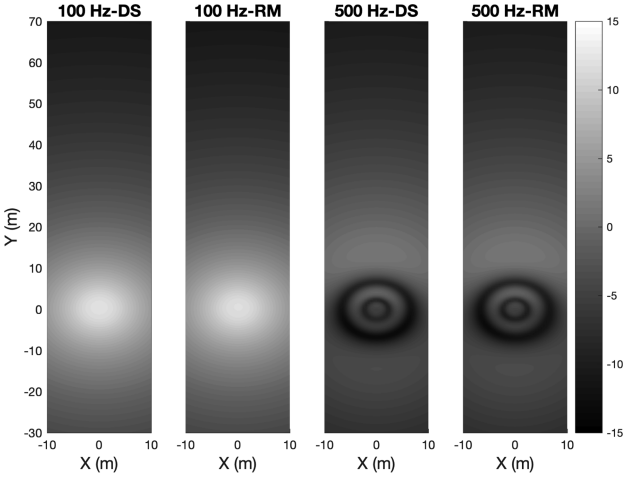

Fig. 10. Relative pressure level referenced to the point of coordinates (0, 20, 0) m. From left to right: direct simulation with Sysnoise at 100 Hz, RM method at 100 Hz, direct simulation with Sysnoise at 500 Hz, RM method at 500 Hz.

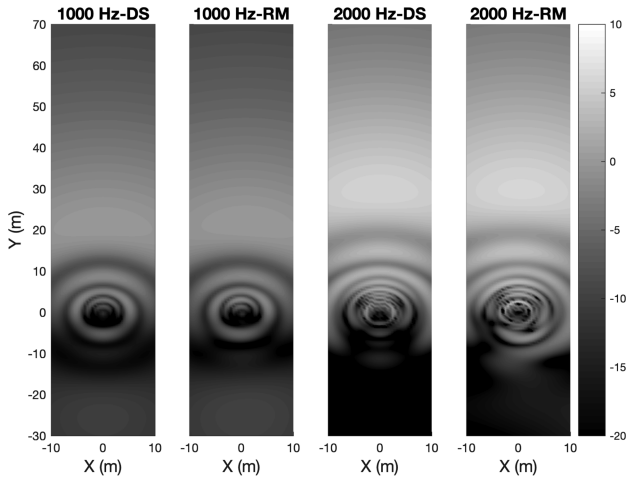

Fig. 11. Relative pressure level referenced to the point of coordinates (0, 20,0) m. From left to right: direct simulation with Sysnoise at 1000 Hz, RM method at 1000 Hz, direct simulation with Sysnoise at 2000 Hz, RM method at 2000 Hz.

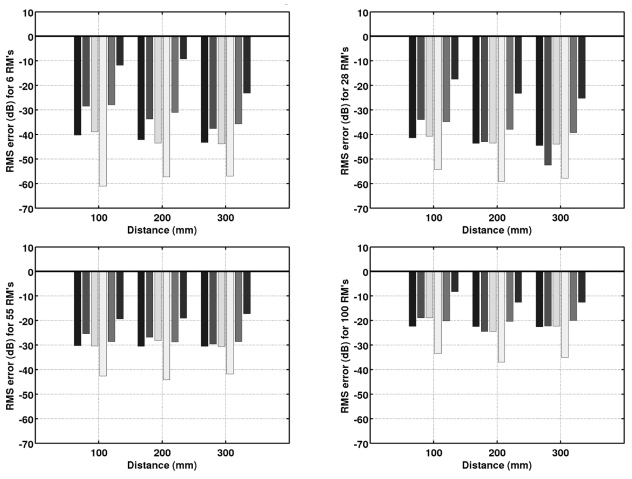

Fig. 12. Error ratio *ERR* at several distances for several frequencies: 100 Hz (upper left), 500 Hz (upper right), 1 kHz (lower left), and 2 kHz (lower right). From left to right, for each distance, the six bars correspond respectively to the following distribution of identification points: all locations, 200 even locations, N_{min} even locations, and N_{min} random locations (min/mean/max *ERR*).

reference (left maps); and the field computed from the RM series identified in the vicinity of the array (right maps). Both results are quite similar up to 1 kHz and reveal minor discrepancies at 2 kHz, mainly behind the line array, where its directivity leads to weak pressures.

These simulations lead to performances similar to those observed in the experimental cases of Sec. 2, which indicates that the main characteristics of the radiated field seem to be reasonably well described when using the RM method with the minimum number N_{min} of RMs estimated from the CE curve. To complete this last example, the next sections will investigate the main parameters of the RM method by means of postprocessing these line array simulations.

3.3 Influence of Identification Locations

In order to compare various parameters, let's now define an error criterion *ERR* as the ratio (expressed in dB) of the weighted RMS error to the weighted RMS pressure, both averaged over an "error zone" including 2419 locations, as defined over the ground for the entire x coordinate (± 10 m) range and for y coordinates between 30 m and 60 m. Figs. 10 and 11 show that the line array exhibits a smooth and even response at all frequencies in this zone (with the suboptimal steering used here). Although not fully representative of the actual line array, this error zone seems to be adequate for the purpose of comparing different situations. Moreover, a spatial weight function W has been introduced so that all locations belonging to the error zone are ascribed similar importance when averaging. The expressions for *ERR* and W are given below:

$$ERR = 10\log\left(\frac{\sum_{y_i=30m}^{y_i=60m} ||W(i)\ (P_{est}(i) - P_{ref}(i))||^2}{\sum_{y_i=30m}^{y_i=60m} ||W(i)\ P_{ref}(i)||^2}\right) \quad (6)$$

with

$$W(i) = \sqrt{x_i^2 + y_i^2 + (z_i - z_0)^2} \quad (7)$$

where: $P_{est}(i)$ is the pressure estimated by the RM method, $P_{ref}(i)$ the pressure initially computed using the Sysnoise code, x_i, y_i, and z_i the coordinates of a location i for comparing the pressure, and $z_0 = 2.5$ m the height of the lower edge of the line array.

The identification locations have been modified by selecting them over three parallelepiped surfaces, thus leading to the sets $C1$, $C2$, and $C3$ surrounding the source, at increasing distances D_i from the parallelepiped enveloping the source body. These surfaces are not conformal since they are not correlated with the actual "step-array" shape of the source; however, their simple geometry does serve to define the distance D_i unambiguously.

The locations over each identification surface have been chosen with relatively even spacing: $8 \sim 10$ cm, which equals about half the smallest dimension of the source body and is smaller than the minimum value for D_i. Table 2 lists, for each identification set, the three corresponding dimensions, the number of locations along each axis, the total number of locations N_{tot}, and the distance D_i.

We next computed the estimation error *ERR* for six test cases with varying identification locations over each of the three identification surfaces. The first test case uses all possible locations over the surface (hence their number increases with D_i, see Table 2). The second test case uses locations evenly distributed over the surface, with the minimum number N_i of locations defined in Sec. 3.2. The third test case uses a fixed set of 200 locations evenly distributed over the surface and identical for each frequency. The next test case uses 500 runs of a random selection of N_i locations over the surface, with no constraint regarding positioning (uniform distribution of the location indices). Three *ERR* values are then given: the minimum, mean, and maximum values obtained during these runs. These *ERR* values are displayed in Fig. 12 (the lower the bar, the better the estimation).

These results show that random sets of N_i locations may outperform the set using all locations, which nonetheless produces a consistent *ERR*, regardless of the distance. Conversely, random sets may also lead to very poor performances, thus emphasizing the importance of selecting a suitable set. Interestingly, an even set of N_i locations leads to performances that tend to approximate the average, therefore allowing it to be considered as a "reasonable" identification set. The case of 200 even locations is also interesting, by virtue of being independent of frequency, which is realistic in practice. This set contains N_i locations at 2 kHz and leads to performances similar to the set using all locations at lower frequencies making it a good candidate, hence its use in subsequent simulations.

Surprisingly, the results in Fig. 12 display the limited influence of distance D_i, even though we chose identification surfaces very close to the source body. This finding seems to contradict the main hypothesis behind the method presented here, which solely relies on a series of propagating RMs. An examination of computed data indeed shows that the pressures at all our identification locations are nearly completely reactive (i.e., out of phase with velocity), thus indicating a strong evanescent field. However, the P_{ref} and P_{est} values are found to be very close to one another, even on surface $C1$, which indicates that our RM expansion is able to accurately estimate this evanescent field (hence explaining that inversion of the $\mathbf{H_i}$ matrix leads to a correct $\mathbf{w}$ vector). One explanation may be that the radiating RMs generate reactive pressure like any other vibration pattern and are already dominant even at the short distances considered herein. This result is interesting since close measurements are less corrupted by noise or reverberation.

3.4 Influence of Noisy Measurements

The next simulations focus on the effect of noise on RM method performance. These simulations are based on the fixed set of 200 locations evenly distributed over surface $C2$, which yielded an *ERR* (without noise) of less than −20 dB at all frequencies.

We once again considered six cases for three levels of noise. The first case is a noise-free reference. The second case simply adds some noise to the VM (with a random phase) whose level adjusts from −20 to −40 dB. The third case involves a multiplicative coefficient, with a random variation around a fixed value, leading to an amplitude error varying between 0.1 and 1.0 dB. The fourth case involves a phase error (multiplicative coefficient with unitary amplitude), with an increasing range comparable to the amplitude error. The last two cases are combinations: first, a multiplicative coefficient with both amplitude and phase errors, then with noise added. Here again, 500 independent runs have been averaged for each case; all these test cases are summarized in Table 3. The results presented in Fig. 13 give the *ERR* values corresponding to the aforementioned test cases.

Let's note that the first case is the same for each noise index. Additive noise seems to exert little influence on the *ERR* criterion, which may explain why the presence of a small amount of reverberant noise does not prevent a correct identification in situ: a signal-to-noise ratio can hardly reach a value as low as 20 dB when identification measurements are being performed at 20 cm from the vibrating body. The three test cases involving a multiplicative coefficient are somewhat surprising: it appears that a systematic amplitude error is much more detrimental than a phase error, which itself seems to be negligible. The combination of two kinds of errors is still dominated by amplitude errors, which emphasizes the need for careful calibration of the identification microphones and moreover justifies the use of a single microphone with a robotized set-up. Note that $ERR \leq -20$ dB at all frequencies for a noise index of up to 2, thus corresponding to the uncertainty associated with a good measurement.

Table 3. Noise used to simulate corrupted measurements

Noise index	1	2	3
None	–	–	–
Additive	−40 dB	−30 dB	−20 dB
Real coef.	0.1 dB	0.3 dB	1.0 dB
Phase	±0.66°	±2.0°	±7.0°
Cmplx coef.	2 val. above	2 val. above	2 val. above
Both	3 val. above	3 val. above	3 val. above

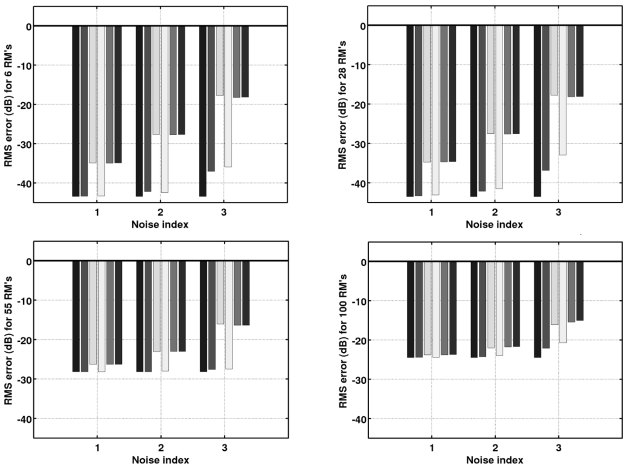

Fig. 13. Error *ERR* with noisy measurements, at 100 Hz (upper left), 500 Hz (upper right), 1 kHz (lower left) and 2 kHz (lower right). For each case, the six bars correspond respectively to the six rows of Table 3.

The noisy simulations presented above lack a test case that corresponds to location errors. This task is not easy using a BEM software, especially our custom package that does not allow changing field points once a solution has been calculated. It is likely that location errors are closer to multiplicative coefficients and, therefore, the source of significant errors. Further work is required to clarify this point.

3.5 Influence of the Number of RMs

A final test has been performed in order to check the validity of the method used to estimate the number of RMs from the CE curve (see Sec. 3.2). The *ERR* criterion has therefore been computed at each frequency with an

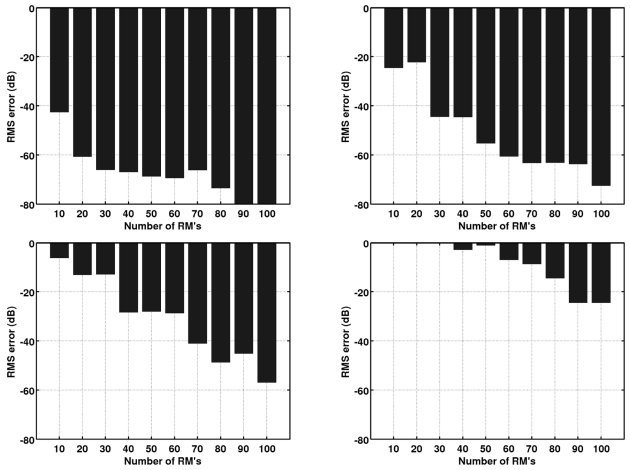

Fig. 14. Relative estimation error with an increasing number of RMs, at: 100 Hz for 6 RMs (upper left), 500 Hz for 28 RMs (upper right), 1 kHz for 55 RMs (lower left), and 2 kHz for 100 RMs (lower right)

increasing number of RMs. We are still considering here 200 identification locations evenly distributed over the $C2$ surface. The corresponding results are presented in Fig. 14 for four frequencies.

At 100 Hz, the CE curve leads to selecting $N = 6$, which yields $ERR \simeq -43$ dB (reference case of Fig. 13). At this frequency, increasing the number N allows significantly reducing the error, to under -80 dB for $N = 100$. Simulations at several frequencies confirm that the minimum number of RMs anticipated from the CE curve lead to estimation errors of less than -30 dB up to 1 kHz. This finding, however, is of little practical effect for end users: a value $ERR = -30$ dB already corresponds to an accuracy that most measurements can hardly achieve with conventional methods. Moreover, the expected gain in accuracy when increasing N is likely to be offset by the effect of any noise or calibration/location errors during the identification, as exposed in Sec. 3.4.

Higher frequencies require both a larger number of RMs and a refined mesh for the BEM model, thus entailing a tremendous CPU cost. Although the RM method might still be usable with a more efficient software, we feel that an expansion requiring more than 100 coefficients is neither practical nor robust. The results presented for 2 kHz, using 100 RMs instead of the minimum 150 anticipated from the CE curve, still lead to a "reasonable" $ERR < -23$ dB, although this is clearly the upper limit of the frequency range over which the RM method may be applied for such a large object.

Moreover, it should be emphasized at this point that the *ERR* criterion has been defined in a zone with a high-pressure level. Although this choice is justified by a normal use of the line array, the *ERR* criterion masks errors in zones with lower pressure levels. Based on our experience, the RM expansion fails to accurately reconstruct the lower pressures of the radiated field.

4 DISCUSSION

From a combination of preliminary numerical computations and a relatively small number of pressure measurements, the estimation method presented here seems to offer a promising tool for estimating the 3D radiation of a source. As an initial assessment step, we presented several examples of RM estimation comparison with actual measurements based on anechoic and in situ identification measurements in considering four small systems of various shapes and configurations. The level of agreement seems to be quite satisfactory, especially when considering the difficulty of anechoic measurements relative to the reduced burden involved for the estimation step. Directivity patterns may indeed be extrapolated (here in a plane, but 3D balloons could also be obtained without any additional measurements).

We feel it would be instructive here to cite the AES2-2012 standard [40]:

> For free-field and half-space measurements, the distance shall, unless otherwise stated, be sufficient to ensure that measurements are made in the far-field of the loudspeaker.
>
> NOTE 1: For large loudspeakers, this may be very difficult to achieve, but there is at present no practical way of using near-field results to reliably derive far-field results, except at low frequencies.
>
> NOTE 2: This does not prohibit the use of other fully described methods of measurement, where the microphone is not in the far-field, which can be shown to produce the same or more accurate result.

Our aim is to propose such a method, which is not as accurate as actual measurements yet seems to offer a very satisfactory tradeoff between practical difficulties and reasonable estimation accuracy. It is however still necessary to assess method performance on numerous practical cases before it can be considered as an attractive alternative.

The measurement examples presented above have been complemented by numerous simulations of a line array with a more complex shape, thus allowing for analysis of the method potential. Once again, we found satisfactory results and showed that the method robustness is promising, at least with respect to the perturbations considered herein. Naturally, this does not mean that the RM method can be considered as the only solution for loudspeaker characterization: it has several drawbacks and limitations, like any estimation method, that will be summarized hereafter.

When based on a model (here a numerical BEM computation), RM method validity is restricted. The body shape must be known with sufficient accuracy (typically better than the mesh scale, i.e., approx. one-tenth of wavelength). This problem is not insurmountable since modern designs involve CAD models that may be converted into a BEM mesh. However, it becomes more difficult to know the microphone locations with great enough accuracy; additional work is still required to assess the practical importance of this point.

A numerical tool is needed to build the RM series, and this may be considered a major obstacle since it

necessitates a skill set not typically found among measurement specialists. Indeed, our custom FELIN software lacks the ease of use of modern commercial software. Conversely, the principle of RM computation is quite simple and may be implemented as an option in most existing codes. Moreover, several alternative methods may be used for the purpose of RM computation. By providing all the required basics surrounding our initial implementation, the aim of this paper has been to promote the development of suitable tools with user-friendly interfaces. As a first step, we are also involved in a public research program intended to release an open-sourced version of the RM computation software.

Even if it were easier to use, the RM method is still limited to a frequency range that does not cover the full audio range. A first frequency limitation is related to the RM computation: higher frequencies involve shorter wavelengths and therefore refined BEM meshes. The CPU time required at higher frequencies becomes prohibitive, even on modern computers. As an example, the line array model presented in Sec. 3 requires 11268 triangular elements to reach about 2 kHz. Using an average modern PC, the RM computation took 2−3 minutes per frequency using our research software. Alternative methods or more efficient implementations may reduce this CPU time significantly; however, it seems unlikely that models much larger than the one presented here could be handled anytime soon. In contrast, the line array case exhibits a very tall shape, thus requiring numerous elements at medium frequencies. Most loudspeaker boxes are more compact, so a usable model size may be valid up to several kilohertz, which may be adequate for many purposes.

Another frequency limitation, which we feel to be even more important, results from radiation physics: at higher frequencies, the complexity of the radiated field increases rapidly with complicated 3D radiation patterns resulting from interferences between different parts of the source body. In order to grasp this complexity, more RMs are needed, requiring more measurements to identify the RM weights. There is still room for improvement in the RM selection and inversion processes, but it seems clear that the RM method requires greater effort at higher frequencies. Even though it is less demanding than actual measurements, the RM method may not be considered a sufficiently efficient alternative at higher frequencies.

We would expect, however, that the frequency range covered for the time being by the RM method already justifies investment in this tool. Compared to other estimation methods, it allows estimating the radiated field with no assumption necessary on the actual vibration pattern or its symmetries. Quick measurements lead to detecting vibrating panels, leakages, etc. Moreover, the RM computation is based solely on body shape, so a single computation may be used to compare design options: alternative or additional drivers, modified ports, etc. We therefore expect the RM method to be an efficient tool at the design stage, during which quick comparisons are more critical than measurement accuracy.

Increasing the number of RMs involved in the estimation process may allow increasing method accuracy. Simulations do tend to show that very good accuracy could be reached in theory, at least up to 1 kHz in the case of the tall line array of Sec. 3. However, increasing the number of RMs requires a greater number of measurements, and their inversion may still be corrupted by noise, reverberation, or diffraction or else by uncertainty over actual measurement locations. The final accuracy may therefore be unsatisfactory and not easily estimated. Also, the RM series tends to describe only coarse notches in the response or directivity, where the radiated pressure is much less than average, which in turn may prevent its use for certain applications (e.g., metrology).

Much work still needs to be done before the RM method may be used routinely. A more exhaustive investigation of the accuracy and robustness of the method is underway based on the simulation of several test cases and a future measurement campaign. This effort should support and further the results presented in Sec. 3 but will not be available before quite some time. In addition, it would be very worthwhile to perform a round-robin comparison between the RM method and other similar estimation/measurement methods. This would also be a large undertaking and should be conducted in partnership with other teams.

5 ACKNOWLEDGMENTS

The authors would like to thank Lucas Vindrola and Clément Vasseur for the measurements conducted on the four speaker systems. The authors also extend their gratitude to the Active Audio company for their interest in this work and especially for providing data on the SA-180 test case.

6 REFERENCES

[1] R. Small, "Simplified Loudspeaker Measurements at Low Frequencies," presented at the *41st Convention of the Audio Engineering Society* (1971 Oct.), convention paper 806.

[2] D. B. (Don) Jr. Keele, "Low-Frequency Loudspeaker Assessment by Nearfield Sound-Pressure Measurement," *J. Audio Eng. Soc.*, vol. 22, no. 3, pp. 154–162 (1974 Apr.).

[3] M. Melon, C. Langrenne, D. Rousseau, and P. Herzog, "Comparison of Four Subwoofer Measurement Techniques," *J. Audio Eng. Soc.*, vol. 55, pp. 1077–1091 (2007 Dec.).

[4] IEC 60268-5, "Sound system equipment—Part 5: Loudspeakers," Standard of the International Electrotechnical Commission (2007).

[5] R. Heyser, "Acoustical Measurements by Time Delay Spectrometry," *J. Audio Eng. Soc.*, vol. 15, no. 4, pp. 370–382 (1967 Oct.).

[6] H. Moller and C. Thomsen, "Electroacoustic Free-Field Measurements in Ordinary Rooms Using Gating Techniques," presented at the *52nd Convention of the Audio Engineering Society* (1975 Oct.), convention paper 1062.

[7] J. Berman and L. Fincham, "The Application of Digital Techniques to the Measurement of Loudspeakers," *J. Audio Eng. Soc.*, vol. 25, pp. 370–384 (1977 Jun.).

[8] D. Rife and J. Vanderkooy, "Transfer-Function Measurement with Maximum-Length Sequences," *J. Audio Eng. Soc.*, vol. 37, pp. 419–444 (1989 Jun.).

[9] M. Dadić, "Wiener Filtering for Anechoic Transfer Function Measurement in Acoustics," *J. Audio Eng. Soc.*, vol. 61, pp. 573–578 (2013 Jul./Aug.).

[10] C. J. Struck and S. F. Temme, "Simulated Free Field Measurements," *J. Audio Eng. Soc.*, vol. 42, pp. 467–482 (1994 Jun.).

[11] J. Backman, "Low-Frequency Extension of Gated Loudspeaker Measurements," presented at the *124th Convention of the Audio Engineering Society* (2008 May), convention paper 7353.

[12] R. Stroud, "Quasi-Anechoic Loudspeaker Measurement Using Notch Equalization for Impulse Shortening," presented at the *129th Convention of the Audio Engineering Society* (2010 Nov.), convention paper 8170.

[13] R. Small, "Closed-Box Loudspeaker Systems. Part I: Analysis," *J. Audio Eng. Soc.*, vol. 20, pp. 798–808 (1972 Oct.).

[14] G. Weinreich and E. B. Arnold, "Method for Measuring Acoustic Radiation Fields," *J. Acoust. Soc. Am.*, vol. 68, no. 2, pp. 404–411 (1980), https://doi.org/10.1121/1.384751.

[15] J. A. S. Angus and M. J. Evans, "Polar Pattern Measurement and Representation with Surface Spherical Harmonics," presented at the *124th Convention of the Audio Engineering Society* (1998 May), convention paper 4717.

[16] F. Fazi, V. Brunel, P.-A. Nelson, L. Hörchens, and J. Seo, "Measurement and Fourier-Bessel Analysis of Loudspeakers Radiation Patterns Using a Spherical Array of Microphones," presented at the *124th Convention of the Audio Engineering Society* (2008 May), convention paper 7354.

[17] M. Melon, C. Langrenne, O. Thomas, and A. Garcia, "Comparison between Measurement and Boundary Element Modelization of Subwoofers," presented at the *127th Convention of the Audio Engineering Society* (2009 Oct.), convention paper 7845.

[18] W. Klippel and C. Bellmann, "Holographic Nearfield Measurement of Loudspeaker Directivity," presented at the *141st Convention of the Audio Engineering Society* (2016 Sep./Oct.), convention paper 9598.

[19] J. Panzer and D. Ponteggia, "Inverse Distance Weighting for Extrapolating Balloon-Directivity-Plots," presented at the *131st Convention of the Audio Engineering Society* (2011 Oct.), convention paper 8473.

[20] H. Lu, S. Wu, and D. B. (Don)Jr. Keele, "High-Accuracy Full-Sphere Electro Acoustic Polar Measurements at High Frequencies using the HELS Method," presented at the *121st Convention of the Audio Engineering Society* (2006 Oct.), convention paper 6881.

[21] M. Melon, C. Langrenne, and P. Herzog, "Evaluation of a Method for the Measurement of Subwoofers in Usual rooms," *J. Acoust. Soc. Am.*, vol. 127, no. 1, pp. 256–263 (2010), https://doi.org/10.1121/1.3270392.

[22] A. Sarkissian, "Acoustic Radiation from Finite Structures," *J. Acoust. Soc. Am.*, vol. 90, no. 1, pp. 574–578 (1991), https://doi.org/10.1121/1.401231.

[23] G. Borgiotti and E. Rosen, "The Determination of the Far Field of an Acoustic Radiator from Sparse Measurement Samples in the Near Field," *J. Acoust. Soc. Am.*, vol. 92, no. 2, pp. 807–818 (1992), https://doi.org/10.1121/1.403951.

[24] M. Sanalatii, P. Herzog, M. Melon, R. Guillermin, J.-C. Le Roux, and N. Poulain, "Measurement of the Frequency and Angular Responses of Loudspeaker Systems Using Radiation Modes," presented at the *141st Convention of the Audio Engineering Society* (2016 Sep.), convention paper 9615.

[25] M. Sanalatii, L. Vindrola, C. Vasseur, P. Herzog, M. Melon, R. Guillermin, N. Poulain, and J.-C. Le Roux, "Assessment of the Radiation Mode Method for In Situ Measurements of Loudspeaker Systems," presented at the *142nd Convention of the Audio Engineering Society* (2017 May), convention paper 9725.

[26] W. Veronesi and J. Maynard, "Digital Holographic Reconstruction of Sources with Arbitrary Shaped Surfaces," *J. Acoust. Soc. Am.*, vol. 85, no. 2, pp. 588–598 (1989), https://doi.org/10.1121/1.397583.

[27] G. Borgiotti, A. Sarkissian, E. Williams, and L. Schuetz, "Conformal Generalized Near-Field Holography for Axisymmetric Geometries," *J. Acoust. Soc. Am.*, vol. 88, no. 1, pp. 199–209 (1990), https://doi.org/10.1121/1.399941.

[28] G. V. Borgiotti, "The Power Radiated by a Vibrating Body in an Acoustic Fluid and its Determination from Boundary Measurements," *J. Acoust. Soc. Am.*, vol. 88, no. 4, pp. 1884–1893 (1990), https://doi.org/10.1121/1.400211.

[29] S. J. Elliott and M. E. Johnson, "Radiation Modes and the Active Control of Sound Power," *J. Acoust. Soc. Am.*, vol. 94, no. 4, pp. 2194–2204 (1993), https://doi.org/10.1121/1.407490.

[30] R. Ohayon and C. Soize, *Structural Acoustics and Vibration* (Academic Press, London, UK, 1998), https://doi.org/10.1016/B978-0-12-524945-4.X5000-2.

[31] P. Herzog, R. Guillermin, P. Lorin, and V. Chritin, "Identification of a Vibration Pattern from Pressure Measurements and Radiation Modes," presented at *EuroNoise* (2015).

[32] H. Wu, W. Jiang, Y. Zhang, and W. Lu, "A Method to Compute the Radiated Sound Power Based on Mapped Acoustic Radiation Modes," *J. Acoust. Soc. Am.*, vol. 135, no. 2, pp. 679–692 (2014), https://doi.org/10.1121/1.4861242.

[33] P.-T. Chen and J. H. Ginsberg, "Complex Power, Reciprocity, and Radiation Modes for Submerged Bodies," *J. Acoust. Soc. Am.*, vol. 98, no. 6, pp. 3343–3351 (1995), https://doi.org/10.1121/1.413821.

[34] J. Zemanek, "Beam Behavior within the Nearfield of a Vibrating Piston," *J. Acoust. Soc. Am.*, vol. 49, no. 1, pp. 181–191 (1971), https://doi.org/10.1121/1.1912316.

[35] P. Herzog and O. Schevin, "Estimation du degré de complexité d'un modèle de source vibrante," presented at the *6th French Acoustic Congress (in French)*, 075 (2002).

[36] G. H. Golub and C. F. V. Loan, *Matrix Computations*, vol. 10 (Physics Today, 1996).

[37] G. Borgiotti and K. Jones, "Frequency Independence Property of Radiation Spatial Filters," *J. Acoust. Soc. Am.*, vol. 96, no. 6, pp. 3516–3524 (1994), https://doi.org/10.1121/1.411407.

[38] M. M. Boone and O. Ouweltjes, "Design of a Loudspeaker System with a Low-Frequency Cardiodlike Radiation Pattern," *J. Audio Eng. Soc.*, vol. 45, pp. 702–707 (1997 Sep.).

[39] X. Meynial, "DGRC Arrays : A Synthesis of Geometrical and Electronic Loudspeaker Arrays," presented at the *120th Convention of the Audio Engineering Society* (2006 May), convention paper 6786.

[40] AES2, "AES standard for acoustics—Methods of measuring and specifying the performance of loudspeakers for professional applications—Drive units," Audio Engineering Society (2012).

[41] S. Kirkup, *The Boundary Element Method in Acoustics* (University of Central Lancashire - online) ISBN 0953403106 (1998).

APPENDIX: THE LMA CUSTOM SOFTWARE

To the best of our knowledge, obtaining the **Z** matrix describing the radiation of a body is not (yet) an option available in commercial software. In order to test the RM method we had to write a custom software, which we named FELIN. Compared to a conventional BEM solver, FELIN does not provide the acoustic field resulting from a given load case but instead explicitly computes the **Z** matrix and expands it. Although we do not consider this software as an actual advancement in the current state of knowledge, it is briefly described here to help the interested reader implement the RM method.

It is possible to establish a relationship between the volume velocities $\mathbf{q_s}$ of each mesh element and the boundary pressures $\mathbf{p_s}$ on this mesh. Such a discretization leads to an impedance matrix **Z** independent of the actual pressure field and capable of being estimated numerically at a given frequency, i.e., using a direct BEM approach as summarized below.

In denoting S as the boundary surface, the pressure p at location M exterior to S (in volume Ω) may be represented by the classical integral formulation:

$$p(\omega, M) = \int_S [\partial_{\mathbf{n}} G(\omega, M, r) p(\omega, r) - G(\omega, M, r) \partial_{\mathbf{n}} p(\omega, r)] \, dS(r) \tag{8}$$

assuming a harmonic solution with $e^{+j\omega t}$ time dependence, G denotes the usual Green function $G(R) = e^{-jkR}/4\pi R$ with $k = \omega/c$ (c the sound speed), and $\partial_{\mathbf{n}}$ denotes the normal derivative (outward normal vector). The acoustic velocity **v** is related to the pressure by $\nabla p = -j\rho\omega\mathbf{v}$, where ρ is the fluid volumetric mass. It is assumed that the computations are not performed at frequencies close to the singularities of the Dirichlet interior problem.

The direct exterior problem may then be discretized over an appropriate (and smooth) mesh so that Eq. (8) is efficiently approximated in assuming piecewise-constant pressures and velocities over the mesh elements. This set-up reduces the continuous integral to a matrix form expressed at the centers of the mesh elements for each value of ω :

$$\frac{1}{2}\mathbf{p_s} = \mathbf{M}\mathbf{q_s} - \mathbf{D}\mathbf{p_s} \tag{9}$$

The impedance matrix **Z** is thus:

$$\mathbf{Z} = \left[\frac{1}{2}\mathbf{I} + \mathbf{D}\right]^{-1} \mathbf{M} \tag{10}$$

where **M** and **D** are computed here using an image source to take the reflective ground into account. The elements of **M** and **D** involve a numerical integration of the Green function over the elements and care must be taken regarding its singularity. Suitable implementation details for this integration step may be found in a reference by Kirkup [41].

The real part of the **Z** matrix is then expanded through a singular-value decomposition as follows:

$$\Re(\mathbf{Z}) = \mathbf{U}\Sigma\mathbf{V}^* \tag{11}$$

where * denotes the matrix transconjugate. Each column of **V** is a real vector of volume velocities on the mesh, while the corresponding column of **U** is a vector of pressures at the element centers. The Σ matrix is a diagonal and contains positive real values. Each RM thus corresponds to a pair of "source" (volume velocity) vector $\mathbf{V_k}$ and "receiver" (pressure) vector $\mathbf{U_k}$ on the mesh, associated with a singular value σ_k representing the radiation efficiency of the corresponding $\mathbf{V_k}$.

The FELIN software has been written in FORTRAN using the NAG scientific library and implements three steps of the RM method, namely: computation of the **Z** matrix, its SVD expansion, and propagation of each **V** column toward the field points, thus building the $\mathbf{H_i}$ and $\mathbf{H_e}$ matrices used in Sec. 2. This was accomplished within a single piece of software in order to avoid storing huge matrices. The FELIN software output is truncated to N_{max} terms for a much smaller amount of data that can be conveniently processed using Matlab functions.

THE AUTHORS


Maryna Sanalatii


Philippe Herzog


Régine Guillermin


Manuel Melon


Nicolas Poulain


Jean-Christophe Le Roux

Maryna Sanalatii received her Master's degree in electroacoustics (IMDEA) in 2014 and Doctorate degree in acoustics in 2018 from Le Mans University, France. Her doctoral dissertation focused on a synthesis of the acoustic field with high spatial contrast. She currently holds the post of Research Engineer at the Le Mans Technology Transfer Center, France.

•

Philippe Herzog graduated in electronic engineering from ENSEA, France, in 1982. From 1983 to 1986 he worked in the aeronautics division of the Crouzet (now Sextant) group, being in charge of developing a compact gyroscope based on an acoustic cavity. He then taught at Le Mans University and received a Ph.D. degree in acoustics from that university in 1987. He spent one year as a postdoctoral researcher in the acoustics group of the University of Sherbrooke (Canada) and joined the French C.N.R.S. state research institute in 1988 as a full-time researcher at the University of Le Mans. He spent two years at C.T.T.M. where he started activities in electroacoustics. In 1998 Philippe joined the Acoustics Laboratory at the Ecole Polytechique Fédérale de Lausanne (EPFL, Switzerland), where he was involved in the active control of noise for power transformers, in collaboration with the ABB group and QuietPower Inc. (New York). From 2000 to 2018 he has been with the Laboratoire de Mécanique et d'Acoustique (C.N.R.S. Marseille), as a senior researcher. He was mainly involved in the development of sound sources and arrays processing for noise control and sound field synthesis. Philippe is author of about 150 scientific papers. He has been president of the French section of the AES (1995–2007), and president of the SFA—the French acoustical society (2014–2017). He is now starting the ARTEAC-LAB engineering company, focused on electroacoustics and sound field control.

•

Régine Guillermin was born in France in 1971. She graduated from the National School of Physics of Marseille, France, in 1996. She received the Ph.D. degree in physics from the the University of the Mediterranean in 2000. Since 2001 she is a Research Engineer at the French National Center for Scientific Research (CNRS) in the Laboratory of Mechanics and Acoustics CNRS UMR 7031, Marseille. Her work is focused on ultrasonic imaging and ultrasonic quantitative characterization for biomedical applications. Another aspect of her work concerns the study of the radiation of vibrating structures by BEM methods. She is a member of the French Acoustical Society (SFA).

•

Manuel Melon was born in France in 1969. He obtained a M.Sc. degree in Le Mans (1992). In 1996 he received his Ph.D. on the ultrasonic characterization of damping materials. Afterwards, Manuel joined the National Engineering Conservatory (Conservatoire National des Arts et Métiers) in Paris as an Associate Professor. In 2014, he was awarded a professorship with full tenure at the Acoustic Laboratory in Le Mans, where he co-supervises the International Master's Degree in ElectroAcoustics (IMDEA). His research emphasis lies in the fields of near-field acoustic holography, electroacoustics, and signal processing. Manuel Melon was the treasurer of the French Acoustical Society from 2004 to 2007 and a long-time member of the SFA electroacoustical group (GEA) board. With GEA and the AES French Section he helped organizing conferences on several topics in electroacoustics. He was inducted as a fellow into the Audio Engineering Society in 2005.

•

Nicolas Poulain was born in France in 1978. He obtained a degree in mechanical engineering in 2001 from Université de Technologie de Compiègne. He joined the Acoustics and Vibrations department at the "Centre de Transfert de Technologie du Mans" that same year as an engineer and became project manager.

•

Jean-Christophe Le Roux was born in France in 1967. He obtained a M.Sc. degree in acoustics in Le Mans (1990). In 1994, he received a Ph.D. degree on the characterization and modelling of electrodynamic loudspeakers. In 1996 he joined the CTTM (Technology Transfer Centre of le Mans) as an engineer in acoustics. CTTM is a SME devoted to technology transfert of research performed at Le Mans University. He is now the head of the acoustic team and works also on electroacoustic developments for industrial applications (test benches).